Lipids in Health and Disease

RESEARCH

Open Access

Untargeted metabolomics and transcriptomics joint analysis of the effects of polystyrene nanoplastics on lipid metabolism in the mouse liver

Lijuan Chen[1,2], Guoyuan Sui[2], Jin Wu[1,2], Ning Li[1,2], Zhe Zhang[1,2], Ying Du[1,2], Meijun Lü[1,2], Xiaorui Yan[1,2], Guowei Pan[3*] and Lianqun Jia[2*]

Abstract

Background Micro/nanoplastics (MNPs), as emerging environmental pollutants, are widely present in environments that are essential for human survival. They exist in vast quantities and possess stable properties, making them challenging to manage. Some reports indicated that there is a positive correlation between the production of MNPs and the incidence of obesity. The liver serves as both the central hub for lipid metabolism and a prime target for MNPs toxicity. These studies revealed that MNPs can lead to increased hepatic lipid accumulation, suggesting that they may be potential obesogens. However, the specific metabolic changes and possible mechanisms involved remain to be elucidated.

Methods This study focuses on the impact of nanoplastics (NPs) on liver lipid metabolism, using C57BL/6J mice (hereinafter referred to as C57 mice) as the research subjects, and exposing them to 100 nm NPs at 1000 μg/L continuously for 12 weeks.

Results The study revealed that (1) NPs led to nondietary weight gain together with an increase in fat volume and mass in mice. (2) NPs significantly increased serum total cholesterol (TC) and low-density lipoprotein cholesterol (LDL-C) levels, with notable differences between groups. Notably, NPs exposure induced opposing effects on serum lipid profiles, elevating high-density lipoprotein cholesterol (HDL-C) concentrations while suppressing triglyceride (TG) levels, though intergroup differences failed to reach statistical significance. (3) NPs caused multiple inflammatory responses in the liver, with significant lipid deposition. (4) Untargeted metabolomics analysis indicated that NPs exposure led to significant alterations in various lipid metabolites, particularly glycerophospholipids. Additionally, transcriptomics reveals that differentially expressed genes (DEGs) triggered by NPs exposure are predominantly involved in metabolic routes including lipid metabolism and cytochrome P450 (CYP). Taken together, these findings suggested that alterations in lipid metabolism resulting from NPs exposure may involve arachidonic acid metabolism.

*Correspondence:
Guowei Pan
panpgw@163.com
Lianqun Jia
jlq-8@163.com

Full list of author information is available at the end of the article

© The Author(s) 2025. **Open Access** This article is licensed under a Creative Commons Attribution-NonCommercial-NoDerivatives 4.0 International License, which permits any non-commercial use, sharing, distribution and reproduction in any medium or format, as long as you give appropriate credit to the original author(s) and the source, provide a link to the Creative Commons licence, and indicate if you modified the licensed material. You do not have permission under this licence to share adapted material derived from this article or parts of it. The images or other third party material in this article are included in the article's Creative Commons licence, unless indicated otherwise in a credit line to the material. If material is not included in the article's Creative Commons licence and your intended use is not permitted by statutory regulation or exceeds the permitted use, you will need to obtain permission directly from the copyright holder. To view a copy of this licence, visit http://creativecommons.org/licenses/by-nc-nd/4.0/.

Phosphatidylcholine (PC) could be the key substance, and the CYP gene family (*Cyp2c23*, *Cyp2c40*) might be the critical genes regulating liver lipid metabolism during NPs exposure.

Conclusions This study has demonstrated that NPs exposure induced obesity and hepatic lipid accumulation in male mice independently of food intake. The integrated omics data identified dysregulated PC metabolism and CYP gene family expression, suggesting their involvement in arachidonic acid-associated pathways. These findings provided preliminary mechanistic clues linking NP exposure to hepatic lipid metabolism dysregulation and helped to elucidate the adverse effects of NPs on liver lipid metabolism.

Keywords Obesogenic factors, Lipid accumulation, Arachidonic acid/metabolism, Phosphatidylcholines, Cytochrome P-450 enzyme system

Introduction

Since the 1950s, plastic products have been widely used in various industries, such as manufacturing, agriculture, and commerce. The unrestrained use of plastic products, indiscriminate social emissions, and high stability have led to increasingly severe plastic pollution in natural environments. Plastic products in the environment degrade into smaller plastic fragments through various physicochemical processes, collectively referred to as MNPs [1], which are further categorized by size: particles sized between 1 μm and 5 mm are considered microplastics (MPs), and those below 1 μm fall into the NPs [2–4]. Among physicochemical parameters, particulate size [5] has been identified as a primary determinant of MNP-associated risks. Generally, MNPs with particle sizes < 150 μm may pass through the intestinal barrier into the body and accumulate, thus MNPs with smaller particle sizes, especially NPs, may pose greater biological risks [6]. Currently, MNPs are widely distributed in different environmental matrixes from which humans can be exposed, such as oceans [7], fresh water [8], soil [9], and air [10]. They are also found in aquatic foods [11], bottled water, sugar, honey, vegetables, fruits, and other dietary items [12], as well as in daily necessities such as facial cleansers and toothpaste. These findings indicate that humans are highly exposed to MNPs.

Human exposure to MNPs occurs predominantly through aqueous food intake, airborne particle inhalation, and cutaneous absorption [13]. Among these routes, ingestion is the primary entry route. Once inside the body, MNPs accumulate in tissues or organs. Numerous studies have indicated that the liver is particularly sensitive to MNPs exposure, which can lead to abnormalities in lipid metabolism within the liver [14, 15]. Previous studies [16] showed that exposure to NPs for 2 weeks caused hepatic steatosis in C57 mice. Lipid metabolic dysfunction refers to the disruption of lipids and their metabolites within the body [17, 18]. In contemporary society, high-fat and high-energy diets can disrupt hepatic lipid homeostasis, and consequently result in the occurrence of metabolic syndrome (MS), metabolic dysfunction-associated fatty liver disease (MAFLD), hyperlipidemia, diabetes, and other chronic metabolic diseases. These chronic metabolic diseases not only have increasing prevalence and incidence rates year by year, but they are also risk factors for various complex critical conditions such as cirrhosis, liver cancer, cardiovascular and cerebrovascular diseases, and malignant tumors outside the liver [19] which seriously threaten people's health and impose significant social and economic burdens. MNPs, as emerging pollutants, may be new risk factors for abnormal lipid metabolism in the liver, a concern that was first raised in marine organisms. Wang et al. [5] revealed through transcriptomics that polystyrene NPs disrupt endoplasmic reticulum protein homeostasis by inhibiting the expression of endoplasmic reticulum-associated degradation genes, thereby inducing lipid metabolism dysfunction and lipid accumulation in the livers of tilapia. Jia et al. [20] elucidated the changes in oyster metabolic profiles, energy metabolism, and inflammatory reaction induced by exposure to polyethylene (PE) and polyethylene terephthalate (PET) MPs through metabolomics. Research [21] indicates that MNPs exhibit a phenomenon of biological magnification, accumulating more in higher organisms through the food chain, which has drawn greater attention from the medical community to the harm and mechanisms of MNPs on mammals. For example, Huang et al. [22] demonstrated through transcriptomics that MPs significantly affect hepatic lipid metabolism of C57 mice by increasing the biosynthesis of unsaturated fatty acids. Moreover, Wang et al. [23] revealed via lipidomics and transcriptomics that MPs exposure leads to changes in hepatic lipid species of C57 mice, with enriched DEGs significantly associated with altered lipid species and metabolic signalling. Although existing researches have mainly examined marine species, MPs, or single-omics approaches, NPs - which accumulate more easily and are more hazardous than MPs - still have many unknowns regarding their effects on mammalian hepatic lipid metabolism and potential mechanisms.

Building upon the previously reported harmful impacts of NPs on lipid metabolism, the present study examined NP-induced alterations in murine lipid metabolism. A

comprehensive untargeted metabolomics approach was employed to profile hepatic metabolic changes following NP exposure, coupled with transcriptomic analysis to elucidate potential mechanisms underlying NP-induced lipid metabolic dysregulation. The investigations identified PC as a pivotal dysregulated metabolite and the CYP gene family (*Cyp2c23*, *Cyp2c40*) as crucial genetic determinants, suggesting the arachidonic acid metabolic pathway may mediate these detrimental effects. This study employed untargeted metabolomics, an analytical platform integrating conventional metabolomics with lipidomics, which enables parallel extraction and reliable detection of both hydrophilic metabolites and lipid components to provide comprehensive metabolic characterization. The specific identification of altered lipid metabolites among the metabolic profiles offers direct evidence for NPs' effects on lipid metabolism. By combining untargeted metabolomics with transcriptomics data, correlations were established between metabolic changes and gene expression patterns through pathway analysis, helping to elucidate previously unclear mechanisms of NP-induced toxicity. The identification of key metabolic perturbations and their potential regulatory mechanisms provides new insights into NPs' hepatotoxic effects on lipid metabolism in mammalian systems.

Materials and methods

Experimental animals

To control for the variable effects of endogenous estrogen on lipid metabolism [24, 25], all experiments used isogenic male C57 mice ($n = 20$) at 8 weeks postnatal age, maintained under pathogen-free (SPF) conditions with controlled body mass (18–22 g). They were purchased from Liaoning Changsheng Biotechnology Co., Ltd. (Experimental Animal Production Licence No. SCXK (Liao) 2020-0001) and housed at the Experimental Animal Center of Liaoning University of Traditional Chinese Medicine (Animal Center Use Licence No. SYXK (Liao) 2019-0004). The environmental temperature of the animal centre was 22 ± 1 °C, with natural lighting and a humidity of 50 ± 5%. The Ethics Committee of Laboratory Animals at Liaoning University of Traditional Chinese Medicine approved the implementation of the experiment. (Approval No. 21000042023008).

Experimental reagents

Polystyrene plastic microspheres (PS-NPs; Big Goose [Tianjin] Technology Co., Ltd., Tianjin, China; FL-PS-R-001); High-fat chow (Xiaoshu Youtai [Beijing] Biotechnology Co., Ltd., Beijing, China); TC (CH0103152), TG (CH0105151), LDL-C (CH0105162), and HDL-C (CH0105161) assay kits (Sichuan Maccura Biotechnology Co., Ltd., Chengdu, Sichuan, China); eosin (GC307021), haematoxylin (GC307020) and oil Red O staining kits (CR2312030) (Wuhan Servicebio Technology Co., Ltd., Wuhan, Hubei, China); Phosphatidylcholine (PC, YJ006201H) Kit (Shanghai Enzyme Linked Biotechnology Co., Ltd., Shanghai, China).

The untargeted metabolomics and transcriptomics analyses were performed by Wuhan MetWare Biotechnology Co., Ltd., Wuhan, Hubei, China.

Grouping, modelling, and sampling

Following a 1-week acclimation period, twenty C57 mice were randomly and evenly divided into a normal control (NC) group and an NPs exposure (NPs) group. Based on literature research [26–28], the NPs group received drinking water containing 1000 μg/L NPs, which was refreshed daily to maintain exposure consistency. Mice had free access to food and water throughout the entire study period. Before sampling, the following model establishment, the weight, dietary intake, abdominal fat volume, and fat mass of the mice were measured for in vivo assessment. Following these measurements, the mice underwent a 12-hour fasting period during which water was provided ad libitum. Then anesthetizing the mice, orbital sinus blood samples were collected and subjected to 2-hour coagulation at room temperature prior to centrifugation (856 ×g, 30 min, 4 °C). Then, the supernatant was stored for future use. After humane euthanasia via cervical dislocation, liver specimens were surgically excised and processed, with half frozen at -80 ℃ and half fixed in 4% paraformaldehyde.

Observation indicators and methods

Characterization of NPs

The NPs dilution was prepared using pure water, with a dilution concentration of 1000 μg/L. The average particle size and dispersity of the NPs stock solution (10 mg/10 mL), NPs dilution, and NPs dilution after 24 h were analyzed using dynamic light scattering (DLS) experiments conducted with the Malvern Zetasizer Nano ZS90 (Malvern Panalytical Ltd., Malvern, UK). All measurements were conducted under controlled conditions (25 °C) using 633 nm excitation light with 90° detection geometry, with triplicate acquisitions per sample.

Body weight and dietary uptake

Use the experimental animal body weight scale (ZK-DST, Henan Zhike Hongrun Environmental Protection Technology Co., Ltd., Zhengzhou, Henan, China) to measure the weight and dietary uptake of mice. The body weights of the experimental animals were measured every two weeks. The daily dietary quantity of mice was calculated as follows [16]. Each group of mice was provided 5 g of feed per mouse per day (50 g of feed per day for every 10 mice). After 24 h, the remaining feed was weighed. The daily dietary quantity of mice was calculated as (50 g

- remaining feed)/10 mice. Measurements were taken every two weeks for three consecutive days and recorded as raw data.

Measurement of abdominal fat volume and total body fat mass

A small animal in vivo MicroCT scanner (QuantumGXII, PerkinElmer, Waltham, MA, USA) was used to measure the total abdominal fat volume below the diaphragm in the mice. Isoflurane was continuously administered to anesthetize the mice. The position of the mouse bed was adjusted to center the abdominal fat image within the CT field of view. Imaging parameters included 90 kV excitation voltage, 80 μA beam current, and 36 μm voxel size, using High Resolution acquisition over 4 min. Abdominal fat images of the mice were obtained, and after secondary reconstruction, the total volumes of visceral and subcutaneous fat in the abdomen were analysed and calculated.

Total body fat content was measured using the EchoMRI-100 H system (EchoMRI LLC, Houston, TX, USA). First, the mouse was weighed and placed in a holder suitable for its weight. Next, the holder containing the mouse was completely inserted into the detection slot of the small animal body composition analyser. The EchoMRI software was used to perform the system test and measure the total body fat content of each mouse. The instrument automatically takes two measurements and calculates the average value.

Determination of mouse liver weights

After the mice were euthanized under anaesthesia, complete hepatic excision was performed, with the organ subsequently placed on weighing paper, a balance was used to weigh it, and the weight was recorded.

Mouse blood lipid testing

An automatic biochemical analyser (7180, Hitachi High-Tech Corporation, Tokyo, Japan) was employed to quantify serum TC, TG, LDL-C, and HDL-C levels.

Histopathological examination of the mouse liver

Slices were prepared using an embedding machine (JB-P5, Wuhan Junjie Electronics Co., Ltd., Wuhan, Hubei, China) and a pathological microtome (RM2016, Leica Biosystems (Shanghai) Co., Ltd., Shanghai, China), and photographed with a digital slide scanning imaging system (Precipoint M8, Precipoint GmbH, Munich, Germany). HE and Oil Red O staining were performed to examine pathological morphology and lipid deposition in liver tissues.

HE staining: Following fixation, liver tissues were dehydrated, cleared in xylene, paraffin-embedded, and sectioned (~5 μm). Take photos and observe after HE staining and covering slides. Oil Red O staining: the fixed liver tissue undergoes sucrose dehydration, OCT embedding, preparation of frozen sections approximately 6 μm thick, immersion in 60% isopropanol, staining with Oil Red O solution for 10 min, followed by mounting, photographing, and observation.

Untargeted metabolomics analysis

Extraction method

Extraction method for hydrophilic substances 20 mg of liver tissue was homogenized and first centrifuged at 1016 ×g, 4 °C for 30 s. Next, 400 μL of a 70% methanol solution containing the internal standard was added, and the suspension was vortexed for five minutes then incubated on ice for fifteen. The sample was then subjected to high-speed centrifugation (16260 ×g, 4 °C, 10 min), after which 300 μL of the clear supernatant was harvested and placed at − 20 °C for half an hour. Following an additional 3-minute spin under the same conditions, 200 μL of the upper phase was retrieved and set aside for downstream analysis.

Hydrophobic substance extraction methods

After homogenizing 20 mg of liver tissue, centrifuge at 1016 (×g) for 30 s at 4 °C. 1 mL of lipid extraction solvent containing the internal standard was introduced to the sample, and the mixture was agitated vigorously for 15 min. Upon the addition of 200 μL of water, the sample was mixed vigorously for one minute and then centrifuged (16,260 ×g, 4 °C, 10 min). 200 μL of the upper clear liquid was removed, and the mixture was evaporated to dryness. 200 μL of lipid reconstitution solution was added, the mixture was vortexed for 3 min, the sample was subjected to a 3-minute, 16 260 × g spin, then the supernatant was removed for analysis.

Chromatography-mass spectrometry data acquisition

Ultra-performance liquid chromatography (UPLC) and tandem mass spectrometry (MS/MS) were used to acquire the metabolomics data.

Hydrophilic interaction liquid chromatography conditions

Chromatographic separation was carried out on a Waters ACQUITY UPLC HSS T3 C18 column (40 °C) at 0.4 mL/min, using water (A) and acetonitrile (B). The gradient ran from 95:5 A/B at 0 min to 10:90 at 11.0 min, held through 12.0 min, returned to 95:5 by 12.1 min, and re-equilibrated until 14.0 min. A 2 μL aliquot was injected.

Hydrophobic liquid chromatography conditions

Chromatographic separation was performed on a Thermo Accucore™ C30 column (2.1 × 100 mm, 2.6 μm) maintained at 45 °C. Mobile phase A consisted of acetonitrile/water (60/40, v/v) with 0.1% formic acid and 10

mmol/L ammonium formate; phase B was acetonitrile/isopropanol (10/90, v/v) containing the same additives. The flow rate was 0.35 mL/min and the injection volume 2 μL. The gradient ran as follows (A:B):0 min, 80:20 → 2 min, 70:30 → 4 min, 40:60 → 9 min, 15:85 → 14 min, 10:90 → 15.5 min, 5:95 (held to 17.3 min) → 17.5 min, 80:20 → 20 min, 80:20.

Mass spectrometry conditions for hydrophilic substances

The electrospray ionization (ESI) temperature of 500 °C was used, with + 5500 V/−4500 V spray voltages for positive and negative modes. The ion source gas I (GSI), ion source gas II (GSII), and ion source gas (CUR) were adjusted to 55, 60, and 25 psi. The collision-activated dissociation (CAD) parameter was set to 'high', and the triple quadrupole (Qtrap) acquired each ion pair according to its optimized declustering potential (DP) and collision energy (CE).

Mass spectrometry conditions for hydrophobic substances

Using ESI at 500 °C with spray voltages of + 5500 V (pos) and − 4500 V (neg), GS1, GS2 and CUR were fixed at 45, 55 and 35 psi. CAD was Medium, and each ion-pair transition in the triple quadrupole (Qtrap) was detected under the optimized DP and CE.

Sample quality control

Three QC samples, created by blending individual sample extracts, were introduced at regular intervals during analysis to verify analytical repeatability. Data quality was evaluated by computing Pearson's correlation among the QC injections; coefficients approaching ± 1 reflected a highly stable detection process and superior data quality.

Transcriptome sequencing analysis

RNA detection

Six samples were randomly selected from each of the NC groups and the NPs groups for RNA quality assessment. RNA integrity and DNA contamination were analysed. RNA concentration was precisely determined with a Qubit 4.0 fluorometer/MD microplate reader. Ultimately, five samples from the NC group and five samples from the NPs group were included in the transcriptome sequencing analysis.

Library construction and quality control

The total RNA pool was subjected to oligo (dT) magnetic-bead capture to isolate mRNA, which was then fragmented using fragmentation buffer. Using the fragmented RNAs as templates, a reverse transcriptase system generated cDNA. The cDNA was subsequently cleaned and subjected to end repair, adenine overhang addition, adapter ligation, fragment size-fractionation, PCR amplification and final purification. Ultimately, the enriched library was obtained through PCR amplification. Once library preparation was complete, an initial concentration measurement was carried out using the Qubit fluorescent dye assay. The library passed quality control when the effective concentration was greater than 2 nM. Upon passing quality checks, the prepared library was run on the Illumina sequencer.

Bioinformatics analysis

Differential gene expression between conditions was analyzed using DESeq2, resulting in the identification of a set of DEGs between the two biological conditions. In order to control the false discovery rate (FDR), *P* value underwent adjustment for multiple comparisons. Genes with $|\log_2$ fold change$| \geq 1$ and FDR < 0.05 were considered differentially expressed. This DEG set was then subjected to clustering analysis, and a heatmap was generated to group genes or samples with similar expression patterns. Functional annotation of the DEGs was performed using Kyoto Encyclopedia of Genes and Genomes (KEGG) pathway analysis.

RT-qPCR to verify the expression of differentially expressed gene mRNA in mouse liver tissue

Using real-time fluorescence quantitative polymerase chain reaction instrument (CFX Opus 96, Bio-Rad Laboratories, Inc., Hercules, CA, USA), water bath constant temperature shaker (SHZ-88, Haimen Kylin-Bell Lab Instruments Co., Ltd., Haimen, Jiangsu, China), and high-precision analytical balance detected differential genes mRNA expression. From 20 mg of liver, total RNA was obtained, quantified, and used for cDNA synthesis via reverse transcription. Amplification conditions were set according to the kit manual. *β-actin* served as the internal reference to quantify the relative mRNA levels of differential liver genes *Cyp2c23* (Mus musculus cytochrome P450 family 2, subfamily c, polypeptide 23), *Cyp2c40* (Mus musculus CYP2C40), and *Cyp2b9* (Mus musculus cytochrome P450 family 2, subfamily b, polypeptide 9). Relative quantification analysis was performed using the 2^-ΔΔCt method. Primers were synthesized by Saiyi Biotechnology Co., Ltd., Beijing, China (Table 1).

ELISA method to verify the PC levels in mouse liver

After letting the PC kit stand at ambient conditions for twenty minutes, samples were added per the protocol and then incubated at 37 °C, washed the plate, and added the reaction substrate, then measured the absorbance at 450 nm, ploted the standard curve for linear regression, and calculated the PC levels in the mouse liver.

Statistical methods

Data analysis and visualization were performed utilizing GraphPad Prism 8 software, with sample sizes indicated

Table 1 Primer sequence

Gene	Primer sequence（5'-3'）	NCBI	Gene ID	Length / bp
Cyp2c23	Forward:5′-TGTCCCTCAGCCTCCTTTCA-3′ Reverse:5′-TGTCCCTTCTGGCTATCTTCG-3′	NM_001167905.1	226143	295bp
Cyp2c40	Forward:5′TGTATGCAGGACAGGAACCAC-3′ Reverse:5′-TGCTGAGAAAGGCACGAAGT-3′	AF047727.1	13099	279bp
Cyp2b9	Forward:5′-GAAGACCCTTCGGCGATTC-3′ Reverse:5′-AGATGATGTTGGCTGTGATGC-3′	NM_010000.2	13094	176bp
β-actin	Forward:5′-GATGGTGGGAATGGGTCAGA-3′ Reverse:5′-GCTGGGGTGTTGAAGGTCTC-3′	EF095208.1	11461	264bp

for each parameter. For inter-group comparisons, statistical comparisons employed an independent t-test when normality assumptions were met, otherwise a Wilcoxon rank-sum test was used; $P<0.05$ denoted significance.

Results

DLS assay

Dynamic light scattering (DLS) measurements indicated that the Z-average of the NPs stock solution was 117.0 nm, with 80% of NPs having a particle size between 88.2 nm and 152 nm, a maximum particle size not exceeding 190 nm, and a PDI of 0.141; after dilution of the NPs solution, the Z-average was 115.5 nm, with 80% of NPs having a particle size between 70.2 nm and 132 nm, a maximum particle size not exceeding 190 nm, and a PDI of 0.292; after 24 h of dilution, the Z-average of the NPs solution was 133.3 nm, with 80% of NPs having a particle size between 86.5 nm and 158 nm, a maximum particle size not exceeding 220 nm, and a PDI of 0.263 (Fig. 1).

Effects of NPs exposure on mouse body weight and daily food intake

The mice remained alive throughout the entire experimental period. In comparison to the NC group, the mice's weight in the NPs group increased with prolonged exposure to NPs. This change became evident from the 6th week of NPs exposure and continued until the end of the experiment. At the 12-week mark, a notable distinction emerged when comparing the two groups ($P<0.05$) (Fig. 2A). Daily food intake of the mice gradually decreased from the 8th week, and the difference between two groups at the 8th and 10th weeks was significant ($P<0.05$) (Fig. 2B). The pattern of body weight increased

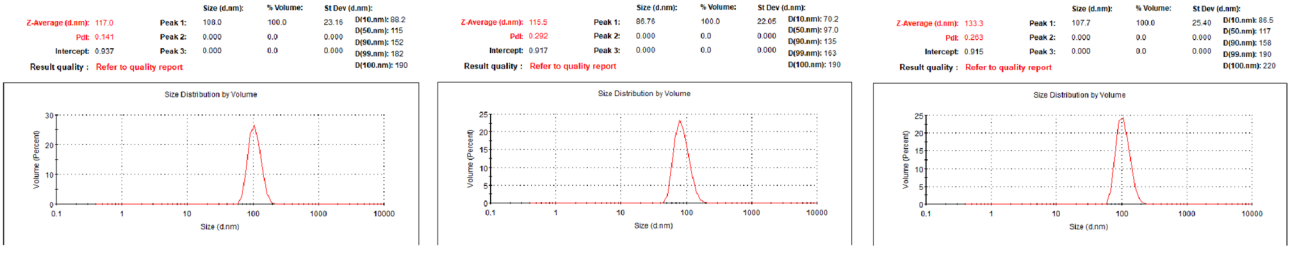

A B C

Fig. 1 Characterization of polystyrene nanoplastics. **A**: DLS data of NPs stock solution (10 mg/10 mL); **B**: DLS data of 0 h-NPs dilution (1000 μg/L); **C**: DLS data of 24 h-NPs dilution (1000 μg/L)

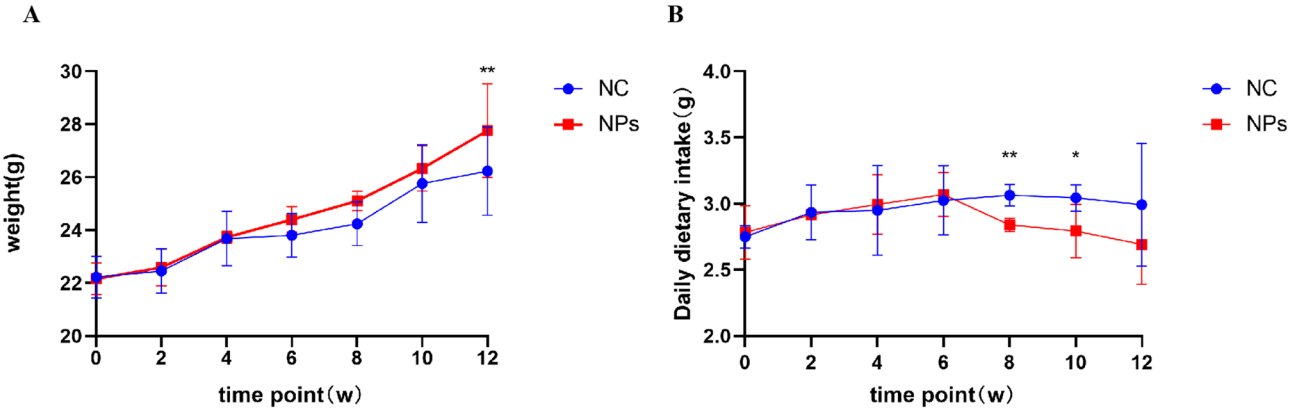

Fig. 2 Changes in body weight and daily food consumption in mice after 12 weeks of NP exposure. **A**: Trend in body weight of mice, t-test, $n = 10$; **B**: Trend in daily food intake of mice, $n = 3$. t-test, * $P < 0.05$, ** $P < 0.01$

together with stable food intake, suggesting that the weight gain in the NPs group was not driven by diet.

Effects of NPs exposure on abdominal fat volume and total body fat mass in mice

Relative to the NC group, after 12 weeks of NPs exposure, the visceral fat and total fat volume below the thorax in the NPs group showed a substantial increase ($P < 0.05$). There was a trend towards increased subcutaneous fat volume, but no statistically meaningful variation was detected among the groups ($P > 0.05$) (Fig. 3A-C). Moreover, compared with the NC group, 12 weeks of NPs exposure significantly increased the whole-body fat content and the total body fat percentage in the mice ($P < 0.05$) (Fig. 3D-F). The findings indicate that the mice's weight gain is attributable to increased fat accumulation.

Effects of NPs exposure on serum lipids, liver histopathology, and lipid deposition in mice

The results indicated that NPs altered mice serum lipid profiles. Specifically, no significant differences in HDL-C or TG were found between the groups ($P > 0.05$) (Fig. 4A and B), whereas the NPs group showed a marked increase in LDL-C and TC relative to the NC group ($P < 0.05$) (Fig. 4C and D). The study also focused on changes in liver weight and hepatosomatic index (HSI) in mice. A trend toward increased liver weight and HSI was observed in the NPs group; however, the differences did not reach statistical significance ($P > 0.05$) (Fig. 4E and F).

H&E staining revealed that in the NC group, the boundaries of hepatic lobules in the mice were distinct, with hepatocytes arranged orderly and densely. The cytoplasm was abundant, and cellular morphology appeared normal. There were no significant abnormalities in the portal areas between adjacent hepatic lobules, and no apparent signs of inflammation were detected. Upon completion of the 12-week NPs exposure period, the hepatic lobules in the mice appeared morphologically normal, and the hepatocyte structure did not significantly change, but the arrangement of hepatocytes was slightly sparser. Inflammatory cell infiltration was observed in several areas (yellow arrows) (Fig. 4G). Oil Red O staining revealed no obvious lipid droplets in the livers of the mice in the NC group, whereas significant red lipid deposits were present in the livers of the mice exposed to NPs for 12 weeks (Fig. 4H). The changes in serum lipid levels, liver weight, and lipid deposition under NPs exposure indicate that NPs provoke disorders of lipid homeostasis within the liver.

Untargeted metabolomics analysis of the mouse liver following NPs exposure

Sample quality control analysis

To evaluate equipment stability and assess the data quality of test samples, three quality control samples (QC) were inserted during the testing process, and QC evaluation relied on the Pearson correlation coefficient. As the absolute value of the correlation coefficient (|r|) approaches 1, the linear association between the variables grows stronger. In this study,|r| was all greater than 0.9, indicating good instrument stability and data reproducibility in this experiment (Fig. 5A).

Screening and analysis of differentially abundant metabolites

The impact of NPs on lipid accumulation in mouse liver was investigated using untargeted metabolomics. Metabolites with fold change>2 and P value<0.05 were preliminarily selected as differentially abundant metabolites between groups. Among the 69 metabolites with changed abundance, 30 exhibited upregulation and 39 exhibited downregulation. On the basis of the primary classification of substances, these differentially abundant metabolites can be divided into 12 categories, with glycerophospholipids being the most abundant (Fig. 5B-D).

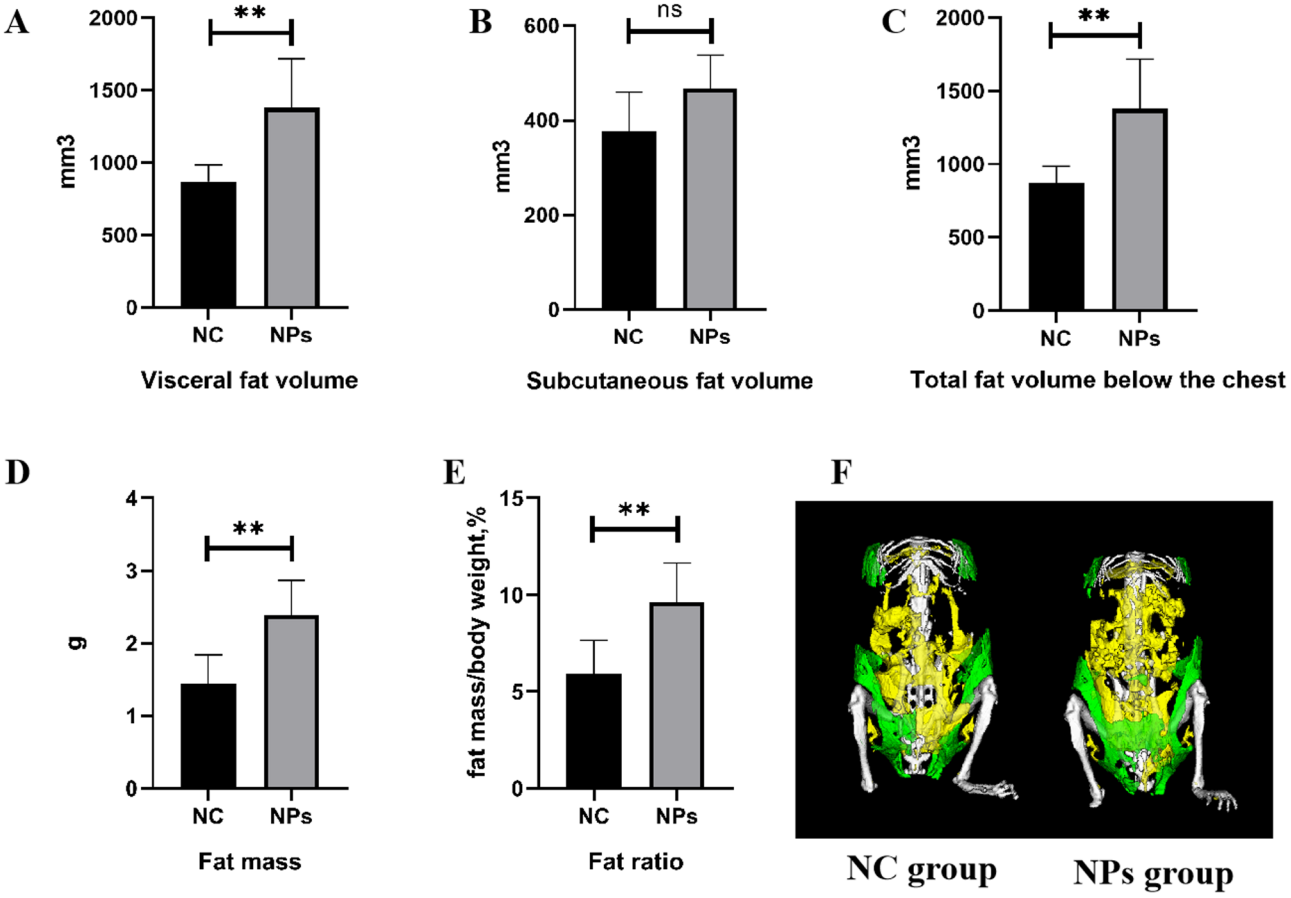

Fig. 3 Changes in fat volume below the rib cage and total body fat mass in mice exposed to NPs for 12 weeks. **A**: Visceral fat volume, t-test, $n=6$; **B**: Subcutaneous fat volume, t-test, $n=6$; **C**: Total fat volume below the rib cage, t-test, $n=6$; **D**: Total body fat mass in mice, t-test, $n=10$; **E**: Percentage of total body fat in mice: fat mass/weight, Wilcoxon rank-sum test, $n=10$; **F**: MicroCT imaging of fat below the rib cage in mice. ns indicates $P>0.05$,* $P<0.05$ and ** $P<0.01$

KEGG enrichment analysis of differentially abundant metabolites

Metabolites can interact with one another, creating metabolic pathways that play important roles in living organisms. Using the KEGG database (Kanehisa et al., 2000) to analyse differentially enriched metabolic pathways, a total of 127 pathways were found to be enriched in the differentially abundant metabolites (Fig. 5E). The five metabolic pathways were collectively enriched 11 differentially abundant metabolites, including 7 glycerophospholipid metabolites and 2 glyceride metabolites. Among the 11 metabolites, 6 were downregulated and 5 were upregulated. The differentially abundant metabolites and the aforementioned five significantly enriched metabolic pathways are shown in Table 2.

Transcriptomic analysis of mouse livers after NPs exposure

Screening and analysis of DEGs

Transcriptomic analysis was performed on mouse liver samples, and DESeq2 was employed to evaluate differential expression between the various sample groups. The selection criteria for identifying differentially expressed genes were established as $|\log_2\text{Fold Change}| \geq 1$ and $P<0.05$. Analysis revealed 327 DEGs, including 222 upregulated genes and 105 downregulated genes (Fig. 6A and B).

KEGG enrichment analysis of differentially expressed genes

KEGG pathway analysis revealed a total of 194 enriched pathways. Among these pathways, 16 enriched pathways were associated ($P<0.05$). The DEGs and the 16 significantly enriched pathways are shown in Figs. 6C-E.

Integrated analysis of untargeted metabolomics and transcriptomics

To investigate the mechanism by which NPs affect metabolites and genes in the mouse liver, untargeted metabolomics and transcriptomics analyses were combined. Based on the KEGG pathway enrichment in the untargeted metabolomics and transcriptomics, two identical KEGG pathways from the two omics studies were selected for mapping, totaling 80 pathways. A bubble

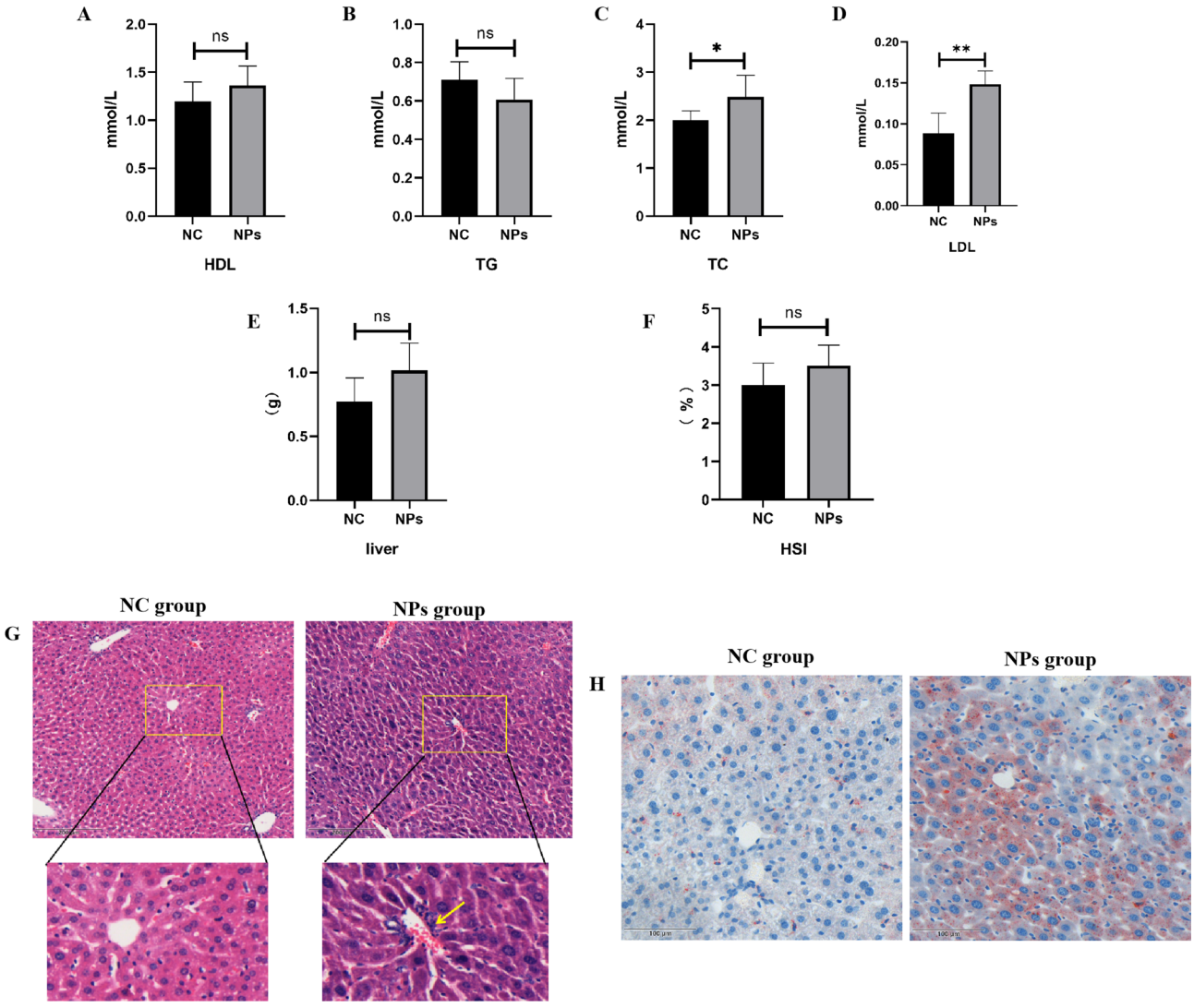

Fig. 4 Impact of NPs on lipid metabolism in the mouse liver. **A**-**D**: Changes in blood lipid levels, $n=6$; **E**: Variation in liver tissue mass, t-test, $n=6$; **F**: Changes in hepatosomatic index (HSI), HSI (%)=(Liver weight (g)/Body weight (g))×100, Wilcoxon rank-sum test, $n=6$; **G**: Changes in the pathological morphology of mouse liver (HE, 200×); H: Lipid deposition in hepatic tissue of mice (Oil Red O, 400×). ns indicates $P>0.05$,* $P<0.05$ and ** $P<0.01$

chart displays the top 25 pathways ranked by *P* value (Fig. 7A). Analysis of these pathways revealed that glycerophospholipid metabolism, linoleic acid metabolism, and arachidonic acid metabolism have a strong association with lipid metabolic functions in the liver. Comprehensive analysis of these three key pathways revealed 17 differentially abundant metabolites, including 1 diglyceride (DG), 5 phosphatidylcholines (PCs), 3 phosphatidylglycerols (PGs), 3 phosphatidylserines (PSs), and 5 lysophosphatidylcholines (LPCs). Among these metabolites, 16 were downregulated, and 1 was upregulated. Additionally, 6 DEGs were identified, namely, *Cyp2c23*, *Cyp2c40*, *Cyp2c70*, *Cyp2b9*, *Etnppl*, and *Phospho1*, with 4 genes downregulated and 2 upregulated (Table 3).

A Pearson correlation analysis of the aforementioned differentially metabolites and genes was conducted, considering an absolute correlation value greater than 0.8 as indicative of a correlation for the two variables, and $P<0.05$ as indicative of a significant correlation. *Cyp2c23* was positively correlated with one PC, three PGs, two PSs, and two PEs, and negatively correlated with one DG. *Etnppl* was positively correlated with three types of PCs, two types of PSs, and one type of PE. *Cyp2c40* was positively correlated with one type of PC. *Phospho1* was positively correlated with one type of PS and two types of PEs. *Cyp2b9* was negatively correlated with three types of PCs, three types of PGs, two types of PSs, and three types of PEs. Finally, *Cyp2c70* showed no obvious correlation with any of the differentially abundant metabolites (Fig. 7B). Further analysis of these correlations revealed that four types of PCs—PC (14:0_20:4), PC (15:0_20:4), PC (18:0_14:1), and PC (22:5_14:1)—are key metabolites

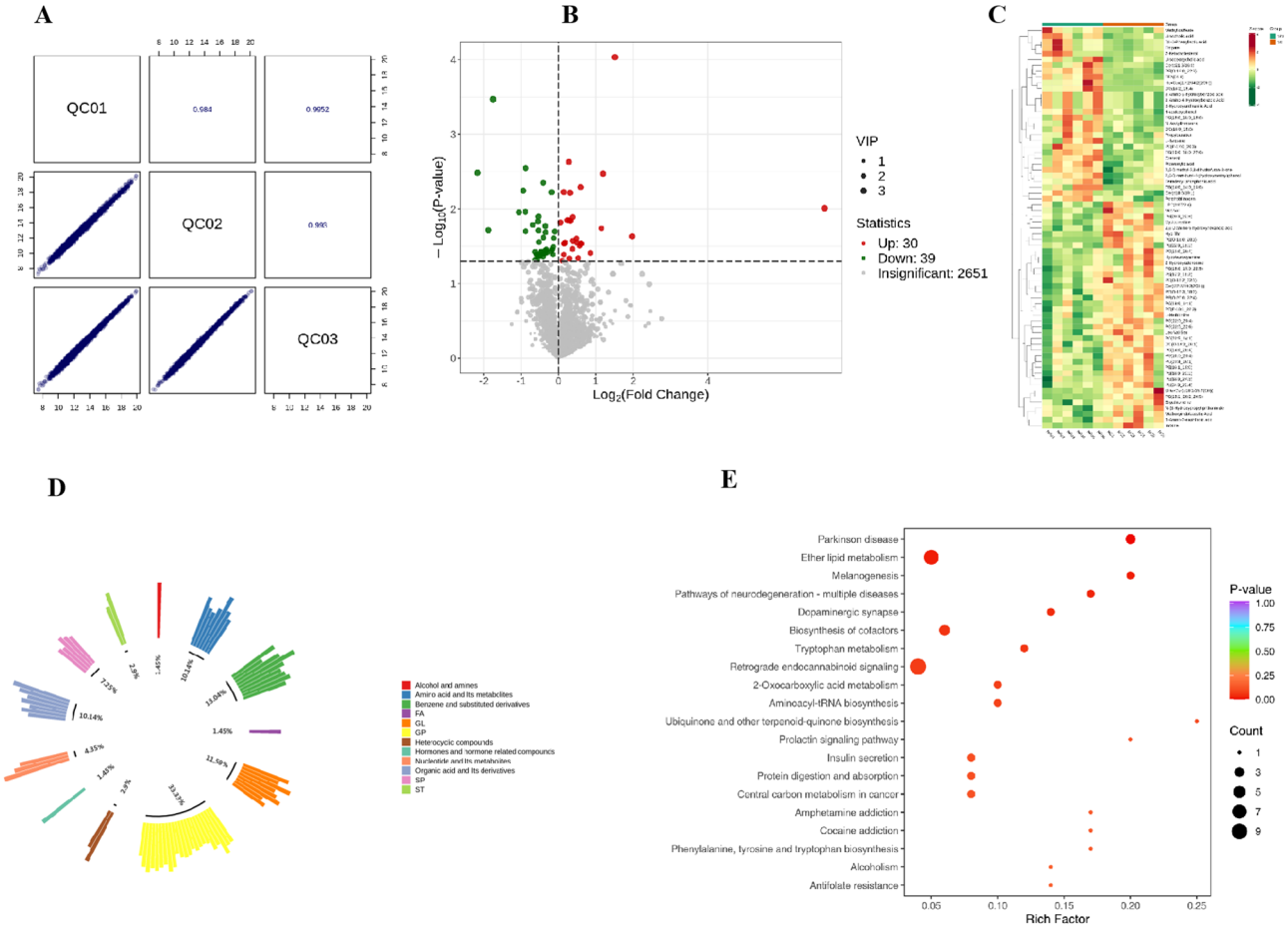

Fig. 5 Untargeted metabolomics analysis of mouse livers after NPs exposure. **A**: QC sample correlation analysis chart; **B**: Volcano plot of differentially abundant metabolites; **C**: Heatmap of differentially abundant metabolites between two groups; **D**: Primary classification of differentially abundant metabolites; **E**: KEGG pathway enrichment bubble chart between two groups, showing the top 20 pathways ranked by *P* value; $n=6$

that are linked with these genes and that these genes are downregulated after NPs exposure. Moreover, pathways associated with glycerophospholipid metabolism, arachidonic acid metabolism, and linoleic acid metabolism pathways were enriched in CYP gene family members (*Cyp2c23*, *Cyp2c40* and *Cyp2b9*). Therefore, these genes may be crucial regulators of liver lipid metabolism in response to NPs (Fig. 8).

Verification of differential metabolites and gene levels by ELISA and RT-qPCR

PC concentrations in the NPs group were markedly reduced relative to the NC group, consistent with the omics results. The mRNA expression of *Cyp2c23* and *Cyp2c40* in the NPs group was significantly decreased compared to that in the NC group, consistent with the omics results; however, the intergroup difference in the mRNA expression level of *Cyp2b9* is not significant (Fig. 9).

Discussion

MNPs, as an emerging environmental pollutant, possess stable properties, degrade slowly, and have lasting and inevitable impacts on humans. Researchers have successively detected MNPs in human faeces [29], sputum [30], breast milk [31, 32], blood [33, 34], and other bodily fluids, as well as in organs such as the lungs [35] and placenta [36]. Earlier investigations [37] have shown that MNPs can persistently deposit in the body throughout an individual's lifetime. This calls attention to the necessity of scrutinizing the negative influences of MNPs on physiological systems and the root causes behind these changes. The liver is the core organ for detoxifying exogenous chemicals and a major target organ for MNPs [15, 38, 39], is also crucial for lipid metabolism in the human body. Thanks to their small size, NPs can more easily lodge in bodily tissues and trigger damage. In this research, we analyzed how NP exposure affects the regulatory circuits of liver lipid metabolism.

In this study, the particle size and dispersion (polydispersity) of NPs were first measured using DLS

Table 2 Differentially abundant metabolites and their statuses in significantly enriched pathways

pathway	Differential metabolites	Fold Change	Type
Parkinson disease	L-Tyrosine	1.23	up
	Piperonylic acid	1.25	up
	DG(16:0_18:0)	1.22	up
Ether lipid metabolism	PE(O-18:0_20:3)	0.30	down
	PE(O-16:0_22:3)	2.85	up
	PE(O-18:2_22:1)	0.75	down
	PE(O-20:0_22:4)	0.78	down
	PE(O-18:3_18:2)	0.62	down
	PE(P-17:0_20:3)	1.41	up
	PE(P-18:1_22:3)	0.52	down
	DG(O-18:2_20:1)	0.54	down
Melanogenesis	L-Tyrosine	1.23	up
	DG(16:0_18:0)	1.22	up
Pathways of neurodegeneration - multiple diseases	Piperonylic acid	1.25	up
	DG(16:0_18:0)	1.22	up
Dopaminergic synapse	L-Tyrosine	1.23	up
	DG(16:0_18:0)	1.22	up

technology. The polydispersity index (PDI) is commonly used to assess the uniformity of particle distribution in a sample. It is generally considered that PDI in the range of 0.05–0.7 is the commonly referenced range in experiments [40], with PDI < 0.3 indicating monodisperse particles with good dispersibility [41]. Using DLS detection, this study found that the PDI of the NPs stock solution, diluted NPs solution, and NPs solution diluted after standing for 24 h were all less than 0.3, confirming their good dispersibility. After standing for 24 h, the average particle size and maximum particle size of the 1000 μg/L NPs solution both slightly increased, suggesting potential aggregation of NPs. In this study, mouse drinking water was replaced daily to ensure their exposure to 100 nm NPs.

The study revealed that NPs exposure affects the metabolic profiles of mice. The results showed that NPs could cause nondietary weight gain in mice by promoting the accumulation of body fat. In 2021, Kannan et al. [42] analyzed official data from the WHO and CDC and found that worldwide plastic output and the global rate of overweight cases have both risen over the last four decades, indicating that MNPs could potentially act as obesogenic agents. This research offers fundamental empirical support for the big data findings of Kannan K et al. Moreover, similar conclusions were reached in studies exploring whether MNPs promote preclinical cardiovascular diseases [43] and in research on risk factors for overweight and excess body weight in children and adolescents [44]. The research then studied NPs' effects on liver lipid metabolism. Exposure to NPs can cause infiltration of inflammatory cells in liver, abnormal blood lipid levels, and significant hepatic lipid deposition. Meanwhile, after NPs exposure, the liver weight and hepatosomatic index (HSI) of mice both exhibited an increasing trend, although there were no significant intergroup differences. However, the increase in HSI is a sensitive indicator of early fatty liver and is directly related to the degree of hepatic lipid accumulation [45]. The induction of liver inflammation by NPs, as exogenous chemical substances, is inevitable and aligns with the findings of several researchers [46–48]. Notably, while the current study did not include the assessment of lipotoxicity markers resulting from hepatic lipid accumulation, subsequent research should evaluate markers including apoptosis and oxidative stress to assess potential lipotoxicity resulting from NP-induced lipid deposition. The effects of MNPs on blood lipid levels exhibit significant variability across studies. For example, Lu et al. [26] observed a reduction in serum TC and TG levels in mice following 5 weeks of exposure to 1000 μg/L MNPs with sizes of 0.5 μm and 5 μm. In contrast, Roh et al. [49] reported elevated serum

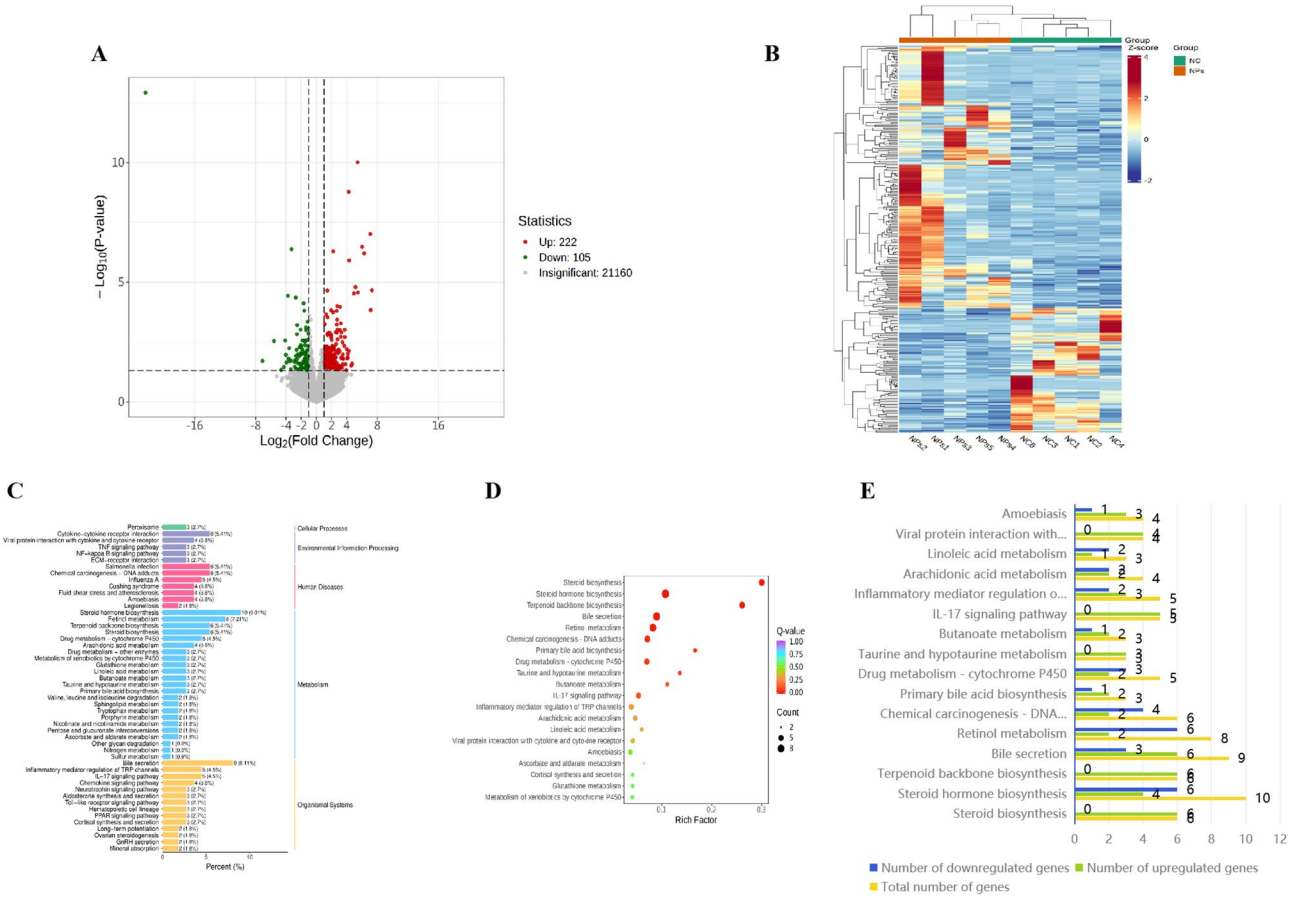

Fig. 6 Transcriptomic analysis of mouse livers after NPs exposure. **A**: Volcano plot of DEGs; **B**: Heatmap of DEGs; **C**: Bar chart of enriched KEGG pathways; **D**: Bubble chart of enriched KEGG pathways; **E**: Number and status of DEGs in significantly enriched KEGG pathways. $n = 5$

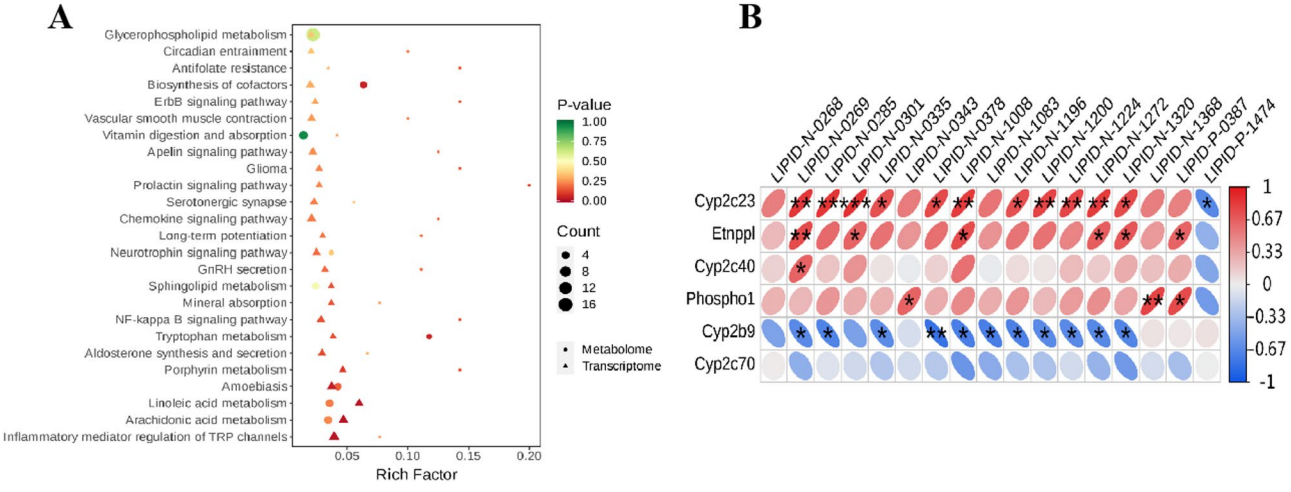

Fig. 7 Integrated analysis of liver untargeted metabolomics and transcriptomics in mice exposed to NPs. **A**: KEGG enrichment bubble plot from integrated untargeted metabolomics and transcriptomics analysis; **B**: Differential metabolite and differential gene correlation analysis diagram. $n = 5$

levels of TG, TC, and LDL-C in mice treated with 100 μg/mL NPs by oral gavage for 9 weeks. In our previous study [16], mice were administered 100 nm NPs at 1000 μg/L for 4 weeks, resulting in a significant decrease in TG levels between groups, while increases in TC, HDL-C, and LDL-C levels were observed without statistically significant differences. In this experimental work, mice were subjected to NPs at the same concentration for 12 weeks.

Table 3 Information on differential metabolites and genes in focused pathways

Differential metabolites or genes	Pathway	Type	Log_2FC	*P* value
PC(14:0_20:4)	Arachidonic acid metabolism Linoleic acid metabolism Glycerophospholipid metabolism	down	-0.532	0.013
PC(15:0_20:4)	Arachidonic acid metabolism Linoleic acid metabolism Glycerophospholipid metabolism	down	-0.342	0.021
PC(20:4_16:1)	Arachidonic acid metabolism Linoleic acid metabolism Glycerophospholipid metabolism	down	-0.548	0.015
PC(22:5_14:1)	Arachidonic acid metabolism Linoleic acid metabolism Glycerophospholipid metabolism	down	-0.877	0.003
PE(16:1_18:0)	Glycerophospholipid metabolism	down	-0.422	0.040
PE(22:0_18:1)	Glycerophospholipid metabolism	down	-0.584	0.041
PE(18:0_24:3)	Glycerophospholipid metabolism	down	-0.310	0.039
PC(18:0_14:1)	Arachidonic acid metabolism Linoleic acid metabolism	down	-0.884	0.011
PE(24:0_20:4)	Glycerophospholipid metabolism	down	-0.359	0.040
PG(20:0_20:4)	Glycerophospholipid metabolism	down	-0.470	0.038
PG(22:0_20:4)	Glycerophospholipid metabolism	down	-0.404	0.024
PG(22:5_22:6)	Glycerophospholipid metabolism	down	-0.490	0.043
PS(18:0_20:1)	Glycerophospholipid metabolism	down	-0.326	0.037
PS(17:2_18:2)	Glycerophospholipid metabolism	down	-0.323	0.035
PS(20:3_22:6)	Glycerophospholipid metabolism	down	-0.189	0.037
LPC(0:0/22:4)	Glycerophospholipid metabolism	down	-0.624	0.048
DG(18:2_18:4)	Glycerophospholipid metabolism	up	7.131	0.010
Cyp2c23	Arachidonic acid metabolism Linoleic acid metabolism	down	-1.005	0.001
Etnppl	Glycerophospholipid metabolism	down	-1.115	0.003
Cyp2c40	Arachidonic acid metabolism Linoleic acid metabolism	down	-1.627	0.019
Phospho1	Glycerophospholipid metabolism	down	-2.672	0.012
Cyp2b9	Arachidonic acid metabolism	up	2.938	0.032
Cyp2c70	Arachidonic acid metabolism Linoleic acid metabolism	up	2.201	0.042

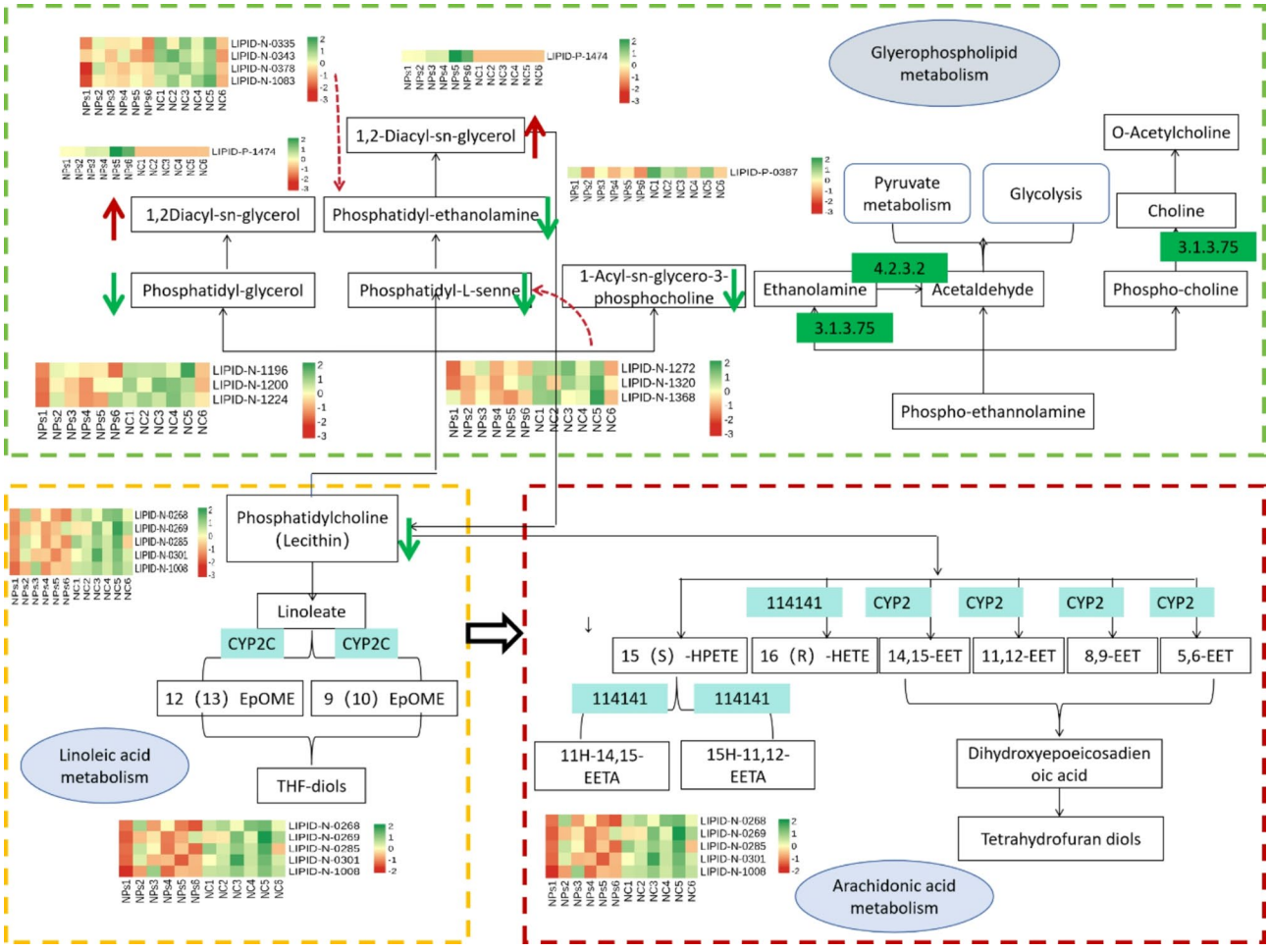

Fig. 8 Analysis of the impact of NPs exposure on lipid metabolism pathways in the liver. In the figure, boxes with solid borders represent differentially abundant metabolites, and boxes without borders represent differential genes. Red arrows indicate metabolites with increased abundance, whereas green arrows indicate metabolites with decreased abundance. The borderless blue boxes indicate genes showing both upregulation and downregulation, while the borderless green boxes denote genes exclusively downregulated

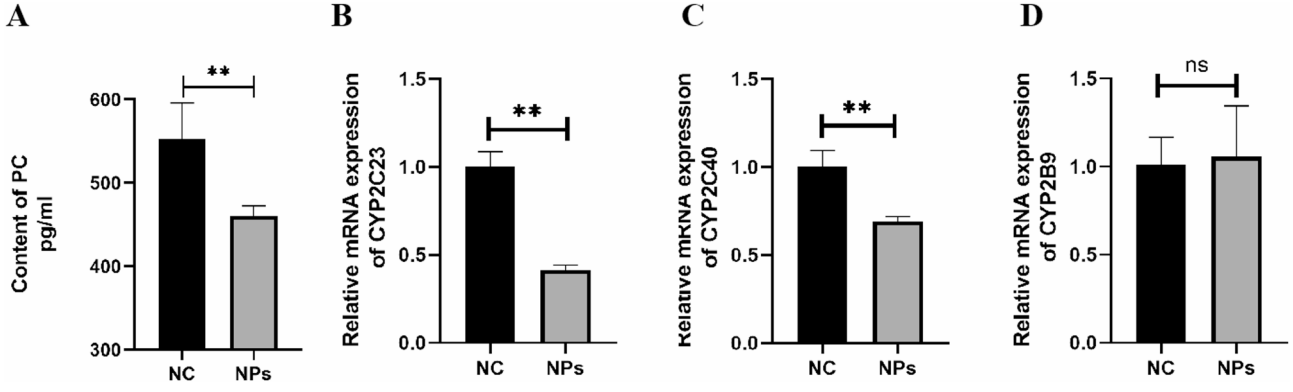

Fig. 9 Verification of differential metabolites and differential gene levels by ELISA and RT-qPCR methods. **A**: ELISA method to verify PC levels, t-test, $n = 5$; **B**-**D**: RT-qPCR method to verify the mRNA expression of *Cyp2c23*, *Cyp2c40*, and *Cyp2b9*, t-test, $n = 5$.ns indicates $P > 0.05$,* $P < 0.05$ and ** $P < 0.01$

The results showed a significant increase in serum LDL-C and TC levels, while HDL-C and TG levels showed no significant differences between groups, although upward and downward trends were observed for HDL-C and TG levels, respectively. These findings are consistent with our earlier observations. The reasons for the differences in blood lipid levels caused by MNPs remain unknown. Further investigations are necessary to determine whether

these differences are associated with the particle size of the MNPs, exposure duration, dose, and other factors. Nevertheless, the hepatic lipid accumulation induced by NPs aligns with the results reported in many previous studies [50–52].

NPs impact lipid metabolism in the body through a complex toxicological process that remains not fully understood, as current studies are still in the early stages. Untargeted metabolomics, as an iterative product of metabolomics, is a combination of traditional metabolomics and lipidomics, providing a comprehensive quantitative detection technique for hydrophilic and hydrophobic metabolites. In this study, high-throughput untargeted metabolomics combined with transcriptomics was applied to comprehensively evaluate the impact and potential mechanisms of NPs on mouse liver metabolism, with lipid metabolites and their pathways being screened, suggesting that hepatic lipid metabolism is one of the key disruption pathways of NPs exposure.

In the untargeted metabolomics analysis, multiple lipid metabolites exhibited significant changes, with GPs showing the most pronounced alterations, accounting for 33.33% of the differentially abundant metabolites. Except for PE (O-16:0_22:3) and PE (P-17:0_20:3), all other GP metabolites were downregulated. KEGG enrichment analysis revealed that five metabolic pathways were significantly enriched in 11 differentially abundant metabolites, seven of which were GP metabolites. All these metabolites were PEs and belonged to the ether lipid metabolism pathway. Consistent with the differentially abundant metabolite analysis results, except for that of PE (O-16:0_22:3) and PE (P-17:0_20:3), the abundance of the other differential GP metabolites included in the KEGG analysis was decreased. Consistent with this study, Liu et al. [53] used lipidomics and reported that in the liver, the lipid subclasses most affected after exposure to MPs were PCs and PEs. Further analysis revealed that after 42 days of low-dose MPs exposure, the abundance of multiple metabolites in the PC and PE subclasses was significantly decreased. GPs are widely distributed in cell membranes and participate in various important physiological functions. They can be further divided into PCs, PEs, PSs, PGs, and lysophosphatidylcholines (LPCs), among others [54]. Among these phospholipids, PCs are the most abundant phospholipid within cells, accounting for 45–55% of the total phospholipids in cells [55, 56]. As a fundamental substance of life, PCs possess various biological properties. Owing to their amphipathic nature, with both lipophilic nonpolar groups and hydrophilic polar groups, PCs are known as natural emulsifiers. They can emulsify cholesterol, thereby reducing cholesterol levels [57, 58], and promote the assembly of very low-density lipoprotein (VLDL) [59], which increases lipid export and subsequently alleviates liver lipid deposition. In addition, PCs prevent inflammasomes from becoming active, resulting in decreased inflammatory cytokines like IL-1β and IL-18, which helps mitigate IL-1β-driven acute and chronic inflammation [60]. PEs are also an important type of GP and are involved in cell membrane construction. They are crucial intermediate metabolites in the arachidonic acid metabolism pathway [61], contributing significantly to the assembly and secretion of VLDL [62] and affecting hepatic lipid metabolism. Transcriptome analysis revealed that NPs exposure altered the hepatic transcriptome profile, with a total of 327 DEGs identified, including 222 upregulated and 105 downregulated genes. The heatmap of differential genes showed individual variations within the group, although the transcriptome data met al.l quality control requirements, possibly reflecting biological differences among individuals. Further KEGG enrichment analysis identified 16 significantly enriched pathways. Among these 16 pathways, more than half may be closely related to lipid metabolic activity in the liver. Numerous studies have examined MNPs' impact on liver lipid metabolism using transcriptomics. By way of example, Yu et al. [63] found that co-exposure to oxytetracycline (OTC) and MNPs of varying sizes markedly alters steroid biosynthesis in zebrafish liver. Similarly, Chen et al. [64] demonstrated that polyvinyl chloride (PVC) MPs modify the spectrum of hepatic metabolites linked to fat metabolism and oxidative-stress defenses. Combined, the studies demonstrate that exposure to MNPs results in abnormalities in liver lipid metabolism.

To focus on the mechanisms by which NPs interfere with liver lipid metabolism, KEGG pathways jointly enriched by untargeted metabolomics and transcriptomics were selected for integrated analysis. The results revealed that glycerophospholipid metabolism, linoleic acid metabolism, and arachidonic acid metabolism have a strong connection with lipid processing in the liver. Four types of PCs may be key substances connecting these three metabolic pathways, and the CYP gene series may be the crucial genes regulating liver lipid metabolism during NPs exposure. In the combined analysis, four types of PCs were downregulated, aligning with Li Y et al.'s findings, which showed a decrease in PC levels following NPs exposure [50]. This could be associated with lipid accumulation in the liver. Moreover, in the joint analysis, changes in the CYP gene family were highlighted. CYP is a conserved protein superfamily present in the membranes of animals, plants, and microorganisms [65]. CYP genes are highly expressed in the liver, where they are involved in processing a variety of internal and external substrates, such as environmental pollutants, drugs, steroids, and fatty acids [66]. MNPs have been reported to cause changes in CYP enzymes or genes in multiple studies, such as the upregulation of *Cyp2p8* expression upon exposure to MPs [67]. Moreover, MPs exacerbate the

inhibition of CYP enzyme activity [68], and the combination of nitrogen and phosphorus compounds and MPs can affect metabolism in organisms through the CYP pathway [69]. The differentially expressed genes induced by MPs in male genitalia have been found to be enriched mainly in the CYP pathway [70]. In this study, it was verified that the CYP series genes involved in lipid metabolism are concentrated in the CYP2C family, specifically *Cyp2c23* and *Cyp2c40*, both of which are significantly downregulated. The CYP2C family is an important P450 subfamily involved in metabolism of endogenous arachidonic acid [71]. This study identified marked decreases in the expression of *Cyp2c23* and *Cyp2c40*, which are typically highly expressed in mouse liver [72, 73]. In the past few decades, studies on *Cyp2c23* have mainly concentrated on the pathways involved in hypertension and hypertensive nephropathy via arachidonic acid metabolism or the mechanisms underlying drug efficacy [74–76]. However, its role in lipid metabolism has not been determined. *Cyp2c40* has been found to metabolize arachidonic acid into hydroxyeicosatetraenoic acids (HETEs) and epoxyeicosatrienoic acids (EETs), with 16 (R)-HETE being the primary metabolite. This metabolite has been shown to act on the vasculature and can inhibit the adhesion and aggregation of neutrophils [77]. Both are intimately involved in arachidonic acid metabolism, which could represent a critical pathway through which NPs disrupt lipid metabolism.

Study strengths and limitations

This study utilized untargeted metabolomics combined with transcriptomics to explore how NPs exposure affects liver lipid metabolism in mice. The analysis identified PC as a key dysregulated metabolite and the CYP gene family (*Cyp2c23*, *Cyp2c40*) as critical genetic regulators underlying NPs-induced metabolic disturbances. Furthermore, mechanistic analysis revealed these effects were potentially mediated through the arachidonic acid metabolic pathway. However, this study has several limitations. First of all, male mice were exclusively used in this study in order to address potential confounding effects of female hormones, which restrict the applicability of the conclusions. Future studies will incorporate female mice and ovariectomized groups to systematically evaluate hormonal and physiological influences on NP-induced toxicity. Secondly, additional mechanistic studies are needed to (1) validate the precise pathways through which NPs interfere with lipid metabolism, and (2) investigate whether and how NPs may exacerbate pre-existing metabolic disorders.

Conclusions

In summary, this study demonstrates that NPs exposure can induce obesity and hepatic lipid accumulation in male mice. Untargeted metabolomics analysis identified lipid metabolites as the most prominently altered metabolic class following NPs exposure. Integrated untargeted metabolomics and transcriptomics analysis suggests this phenomenon may be driven by combined effects on PC metabolism and CYP gene expression, which are closely associated with arachidonic acid metabolic pathways. This study preliminarily revealed the potential mechanisms by which NPs exposure may induce hepatic lipid deposition in male mice through alterations in lipid metabolism, providing new insights into the hepatotoxic effects of NPs. These findings also offer a novel research direction for the prevention and control of related diseases in highly exposed populations.

Supplementary Information

The online version contains supplementary material available at https://doi.org/10.1186/s12944-025-02613-7.

Supplementary Material 1

Acknowledgements

The authors thank Wuhan MetWare Biotechnology Co., Ltd. for the untargeted metabolomics and transcriptomics analyses.

Author contributions

L. C. and L. J. designed the study. G. S., N. L., and Z. Z. designed the experiments. L. C., J. W., Y. D., M. L., and X. Y. conducted the experiments and performed the data analysis. L. C., L. J., and G. P. conceptualized the manuscript, which was written by L. C. All the authors reviewed the manuscript.

Funding

This research was funded by the National Natural Science Foundation of China (82204949), the Joint Program of the Science and Technology Plan of Liaoning Province (2023-MSLH-192), the General Program of the Liaoning Provincial Department of Education (JYTMS20231813), the University Basic Scientific Research Reserve Projects of Liaoning Provincial Department of Education (2024-JYTCB-013), and the Open Fund of the Key Laboratory of the Ministry of Education for TCM Viscera-State Theory and Applications, Liaoning University of Traditional Chinese Medicine (No. zyzx2008).

Data availability

No datasets were generated or analysed during the current study.

Declarations

Competing interests

The authors declare no competing interests.

Author details

[1]Key Laboratory of Ministry of Education for TCM Viscera-State Theory and Applications, Liaoning University of Traditional Chinese Medicine, Shenyang, Liaoning 110847, China
[2]Liaoning University of Traditional Chinese Medicine, Shenyang, Liaoning 110847, China
[3]China Medical University, Shenyang, Liaoning 110122, China

Received: 11 December 2024 / Accepted: 15 May 2025
Published online: 29 May 2025

References

1. Weng Dan H, Shuxian Z. Research progress on the effects of Micro-Nanoplastics on metabolism and their molecular mechanisms [J]. J Hainan Univ (Natural Sci Edition). 2024;42(03):278–89. https://doi.org/10.15886/j.cnki.hdxbzkb.2023070301.
2. Thompson Richard C, Olsen Ylva, Mitchell Richard P, et al. Lost at Sea: where is all the plastic [J]. Science. 2004;304(5672):838. https://doi.org/10.1126/science.1094559.
3. Gigault Julien HA, Ter B, Magalie, et al. Current opinion: what is a nanoplastic [J]. Environ Pollut. 2018;235:1030–4. https://doi.org/10.1016/j.envpol.2018.01.024.
4. Li J, Liu H, Chen JP. Microplastics in freshwater systems: a review on occurrence, environmental effects, and methods for microplastics detection. Water Res. 2018;137:362–74. https://doi.org/10.1016/j.watres.2017.12.056.
5. Wang W, Mao X, Zhang R, Zhou XX, Liu Y, Zhou H, Jia J, Yan B. Nanoplastic exposure at environmental concentrations disrupts hepatic lipid metabolism through oxidative stress induction and Endoplasmic reticulum homeostasis perturbation. Environ Sci Technol. 2023;57:14127–37. https://doi.org/10.1021/acs.est.3c02769.
6. EFSA Panel on Contaminants in The Food Chain. Presence of microplastics and nanoplastics in food, with particular focus on seafood. EFSA J. 2016;14:e04501. https://doi.org/10.2903/j.efsa.2016.4501.
7. Peng G, Bellerby R, Zhang F, Sun X, Li D. The Ocean's ultimate trashcan: Hadal trenches as major depositories for plastic pollution. Water Res. 2020;168:115121. https://doi.org/10.1016/j.watres.2019.115121.
8. Xu S, Ma J, Ji R, Pan K, Miao AJ. Microplastics in aquatic environments: occurrence, accumulation, and biological effects. Sci Total Environ. 2020;703:134699. https://doi.org/10.1016/j.scitotenv.2019.134699.
9. Rillig MC, Bonkowski M. Microplastic and soil protists: a call for research. Environ Pollut. 2018;241:1128–31. https://doi.org/10.1016/j.envpol.2018.04.147.
10. Galvão LDS, Fernandes EMS, Ferreira RR, Rosa DDS, Wiebeck H. Critical steps for microplastics characterization from the atmosphere. J Hazard Mater. 2022;424:127668. https://doi.org/10.1016/j.jhazmat.2021.127668.
11. Jin M, Wang X, Ren T, Wang J, Shan J. Microplastics contamination in food and beverages: direct exposure to humans. J Food Sci. 2021;86:2816–37. https://doi.org/10.1111/1750-3841.15802.
12. Enyoh CE, Shafea L, Verla AW, Verla EN, Qingyue W, Chowdhury T, Paredes M. Microplastics exposure routes and toxicity studies to ecosystems: an overview. Environ Anal Health Toxicol. 2020;35:e2020004. https://doi.org/10.5620/eaht.e2020004.
13. Cheng W, Zhou Y, Chen H, Wu Q, Li Y, Wang H, Feng Y, Wang Y. The iron matters: aged microplastics disrupted the iron homeostasis in the liver organoids. Sci Total Environ. 2024;906:167529. https://doi.org/10.1016/j.scitotenv.2023.167529.
14. Yang X, Jiang J, Wang Q, Duan J, Chen N, Wu D, Xia Y. Gender difference in hepatic AMPK pathway activated lipid metabolism induced by aged polystyrene microplastics exposure. Ecotoxicol Environ Saf. 2022;245:114105. https://doi.org/10.1016/j.ecoenv.2022.114105.
15. Cheng W, Li X, Zhou Y, Yu H, Xie Y, Guo H, Wang H, Li Y, Feng Y, Wang Y. Polystyrene microplastics induce hepatotoxicity and disrupt lipid metabolism in the liver organoids. Sci Total Environ. 2022;806:150328. https://doi.org/10.1016/j.scitotenv.2021.150328.
16. Gao X, Gao J, Zhu J, et al. Effects of polystyrene microplastics on growth, development, and liver lipid metabolism in mice. Chin J Tissue Eng Res. 2024;28:4634–8.
17. Liu Y, Wu Y, Zhang G. Research progress on food-derived polysaccharides alleviating lipid metabolism disorders. Food Res Dev. 2023;44:210–7.
18. Goh GBB, McCullough AJ. Natural history of nonalcoholic fatty liver disease. Dig Dis Sci. 2016;61:1226–33. https://doi.org/10.1007/s10620-016-4095-4.
19. Zeng J, Fan J. Research progress on the natural history of metabolism-associated fatty liver disease. Pract J Liver Dis. 2023;26:769–72.
20. Teng Jia Z, Jianmin Z, Xiaopeng, et al. Toxic effects of exposure to microplastics with environmentally relevant shapes and concentrations: accumulation, energy metabolism and tissue damage in oyster Crassostrea gigas[J]. Environ Pollut. 2021;269:116169.
21. Zuri Giuseppina K, Angeliki, Lacorte Sílvia. Microplastics: human exposure assessment through air, water, and food [J]. Environ Int. 2023;179:108150.
22. Huang H, Wei F, Qiu S, Xing B, Hou J. Polystyrene microplastics trigger adiposity in mice by remodeling gut microbiota and boosting fatty acid synthesis. Sci Total Environ. 2023;890:164297. https://doi.org/10.1016/j.scitotenv.2023.164297.
23. Wang Q, Wu Y, Zhang W, Shen T, Li H, Wu J, Zhang L, Qin L, Chen R, Gu W, Sun Q, Liu C, Li R. Lipidomics and transcriptomics insight into impacts of microplastics exposure on hepatic lipid metabolism in mice. Chemosphere. 2022;308:136591. https://doi.org/10.1016/j.chemosphere.2022.136591.
24. Haibin Z, Jun W, Xuanyi W, et al. Proinflammatory properties and lipid disturbance of polystyrene microplastics in the livers of mice with acute colitis [J]. Sci Total Environ. 2020;750:143085. https://doi.org/10.1016/j.scitotenv.2020.143085.
25. Lonardo Amedeo N, Fabio B, Stefano, et al. Sex differences in nonalcoholic fatty liver disease: state of the Art and identification of research gaps [J]. Hepatology. 2019;70(4):1457–69. https://doi.org/10.1002/hep.30626.
26. Lu L, Wan Z, Luo T, Fu Z, Jin Y. Polystyrene microplastics induce gut microbiota dysbiosis and hepatic lipid metabolism disorder in mice. Sci Total Environ. 2018;631–2. https://doi.org/10.1016/j.scitotenv.2018.03.051.
27. Luo T, Zhang Y, Wang C, et al. Maternal exposure to different sizes of polystyrene microplastics during gestation causes metabolic disorders in their offspring [J]. Environ Pollut. 2019;255(Pt 1):113122. https://doi.org/10.1016/j.envpol.2019.113122.
28. Okamura Takuro H, Masahide H, Yuka, et al. Oral exposure to polystyrene microplastics of mice on a normal or High-Fat diet and intestinal and metabolic Outcomes[J]. Environ Health Perspect. 2023;131(2):27006. https://doi.org/10.1289/EHP11072.
29. Zhang N, Li YB, He HR, Zhang JF, Ma GS. You are what you eat: microplastics in the feces of young men living in Beijing, sci. Total Environ. 2021;767:144345. https://doi.org/10.1016/j.scitotenv.2020.144345.
30. Na J, Geng Y, Jiang Y, et al. Analysis of microplastic pollution in sputum and nasal irrigation fluids of couriers. Chin J Public Health. 2021;37:451–4.
31. Ragusa A, Notarstefano V, Svelato A, Belloni A, Gioacchini G, Blondeel C, Zucchelli E, De Luca C, D'Avino S, Gulotta A, Carnevali O, Giorgini E. Raman microspectroscopy detection and characterisation of microplastics in human breastmilk. Polymers. 2022;14:2700. https://doi.org/10.3390/polym14132700.
32. Liu S, Guo J, Liu X, Yang R, Wang H, Sun Y, Chen B, Dong R. Detection of various microplastics in placentas, meconium, infant feces, breastmilk and infant formula: a pilot prospective study, sci. Total Environ. 2023;854:158699. https://doi.org/10.1016/j.scitotenv.2022.158699.
33. Wu D, Feng Y, Wang R, Jiang J, Guan Q, Yang X, Wei H, Xia Y, Luo Y. Pigment microparticles and microplastics found in human thrombi based on Raman spectral evidence. J Adv Res. 2023;49:141–50. https://doi.org/10.1016/j.jare.2022.09.004.
34. Rotchell JM, Jenner LC, Chapman E, Bennett RT, Bolanle IO, Loubani M, Sadofsky L, Palmer TM. Detection of microplastics in human saphenous vein tissue using MFTIR: a pilot study. PLoS ONE. 2023;18:e0280594. https://doi.org/10.1371/journal.pone.0280594.
35. Wang S, Lu W, Cao Q, Tu C, Zhong C, Qiu L, Li S, Zhang H, Lan M, Qiu L, Li X, Liu Y, Zhou Y, Liu J. Microplastics in the lung tissues associated with blood test index. Toxics. 2023;11:759. https://doi.org/10.3390/toxics11090759.
36. Ragusa A, Svelato A, Santacroce C, Catalano P, Notarstefano V, Carnevali O, Papa F, Rongioletti MCA, Baiocco F, Draghi S, D'Amore E, Rinaldo D, Matta M, Giorgini E. Plasticenta: first evidence of microplastics in human placenta. Environ Int. 2021;146:106274. https://doi.org/10.1016/j.envint.2020.106274.
37. Nor NHM, Kooi M, Diepens NJ, Koelmans AA. Lifetime accumulation of microplastic in children and adults. Environ Sci Technol. 2021;55:5084–96. https://doi.org/10.1021/acs.est.0c07384.
38. Deng Y, Zhang Y, Lemos B, Ren H. Tissue accumulation of microplastics in mice and biomarker responses suggest widespread health risks of exposure. Sci Rep. 2017;7:46687. https://doi.org/10.1038/srep46687.
39. Zhao Y, Bao Z, Wan Z, Fu Z, Jin Y. Polystyrene microplastic exposure disturbs hepatic glycolipid metabolism at the physiological, biochemical, and transcriptomic levels in adult zebrafish. Sci Total Environ. 2020;710:136279. https://doi.org/10.1016/j.scitotenv.2019.136279.
40. Wang L, Zhang J. Li. Advances in dynamic light scattering for nanoparticle characterization [J]. Anal Chem. 2023;95(15):1234–45. https://doi.org/10.1021/acs.analchem.3c01234.
41. Breisch Marina O, Mateusz L, Kateryna, et al. Cell-Biological response and Sub-Toxic inflammatory effects of titanium dioxide particles with defined polymorphic phase, size, and Shape[J]. Nanomaterials. 2023;13(10). https://doi.org/10.3390/nano13101621.
42. Kannan K, Vimalkumar K. A review of human exposure to microplastics and insights into microplastics as obesogens. Front Endocrinol. 2021;12:724989. https://doi.org/10.3389/fendo.2021.724989.
43. Zhao J, Gomes D, Jin L, Mathis SP, Li X, Rouchka EC, Bodduluri H, Conklin DJ. O'Toole, polystyrene bead ingestion promotes adiposity and cardiometabolic

disease in mice. Ecotoxicol Environ Saf. 2022;232:113239. https://doi.org/10.1016/j.ecoenv.2022.113239.
44. Jeong B, Kim JS, Kwon AR, Lee J, Park S, Koo J, Lee W, Baek JY, Shin WH, Lee JS, Jeong J, Kim WK, Jung CR, Kim NS, Cho SH, Lee DY. Maternal nanoplastic ingestion induces an increase in offspring body weight through altered lipid species and microbiota. Environ Int. 2024;185:108522. https://doi.org/10.1016/j.envint.2024.108522.
45. WANG X, ZHANG Y, LI H, et al. High-fat diet induces liver steatosis and early dysmetabolism in mice: association with elevated hepatosomatic index and hepatic lipid accumulation[J]. J Nutr Biochem. 2020;85:108423. https://doi.org/10.1016/j.jnutbio.2020.108423.
46. Zhang K, Yang J, Chen L, He J, Qu D, Zhang Z, Liu Y, Li X, Liu J, Li J, Xie X, Wang Q. Gut microbiota participates in polystyrene microplastics-induced hepatic injuries by modulating the gut–liver axis. ACS Nano. 2023;17:15125–45. https://doi.org/10.1021/acsnano.3c04449.
47. Zhao L, Shi W, Hu F, Song X, Cheng Z, Zhou J. Prolonged oral ingestion of microplastics induced inflammation in the liver tissues of C57BL/6J mice through polarization of macrophages and increased infiltration of natural killer cells. Ecotoxicol Environ Saf. 2021;227:112882. https://doi.org/10.1016/j.ecoenv.2021.112882.
48. Djouina M, Waxin C, Dubuquoy L, Launay D, Vignal C, Body-Malapel M. Oral exposure to polyethylene microplastics induces inflammatory and metabolic changes and promotes fibrosis in mouse liver. Ecotoxicol Environ Saf. 2023;264:115417. https://doi.org/10.1016/j.ecoenv.2023.115417.
49. Roh Y, Kim J, Song H, Seol A, Kim T, Park E, Park K, Lim S, Wang S, Jung Y, Kim H, Lim Y, Hwang D. Impact of the oral administration of polystyrene microplastics on hepatic lipid, glucose, and amino acid metabolism in C57BL/6Korl and C57BL/6-Lep (em1hwl)/Korl mice. Int J Mol Sci. 2024;25:4964. https://doi.org/10.3390/ijms25094964.
50. Li Y, Teng M, Zhao L, Sun J, Yan J, Zhu W, Wu F. Vitamin D modulates disordered lipid metabolism in zebrafish (Danio rerio) liver caused by exposure to polystyrene nanoplastics. Environ Int. 2023;182:108328. https://doi.org/10.1016/j.envint.2023.108328.
51. Lai W, Xu D, Li J, Wang Z, Ding Y, Wang X, Li X, Xu N, Mai K, Ai Q. Dietary polystyrene nanoplastics exposure alters liver lipid metabolism and muscle nutritional quality in carnivorous marine fish large yellow croaker (Larimichthys crocea). J Hazard Mater. 2021;419:126454. https://doi.org/10.1016/j.jhazmat.2021.126454.
52. Du J, Hu Y, Hou M, Zhou J, Xiang F, Zheng H, Zhang X, He X, Xiao H. Combined effects of high-fat diet and polystyrene microplastic exposure on microplastic bioaccumulation and lipid metabolism in zebrafish. Fish Shellfish Immunol. 2023;137:108803. https://doi.org/10.1016/j.fsi.2023.108803.
53. Liu M, Mu J, Wang M, Hu C, Ji J, Wen C, Zhang D. Impacts of polypropylene microplastics on lipid profiles of mouse liver uncovered by lipidomics analysis and Raman spectroscopy. J Hazard Mater. 2023;458:131918. https://doi.org/10.1016/j.jhazmat.2023.131918.
54. Farese RV, Walther TC. Glycerolipid synthesis and lipid droplet formation in the Endoplasmic reticulum. Cold Spring Harb Perspect Biol. 2023;15:a041246. https://doi.org/10.1101/cshperspect.a041246.
55. Jiang Y, Chen J, Li X, et al. Biological functions of phosphatidylcholine and its role in cardiovascular diseases. Chem Life. 2022;42:412–23.
56. Huang Y, Zhong Y. Study on the stability of phosphatidylcholine in soybean lecithin. J Food Saf Qual. 2017;8:4827–31.
57. Cao P, Wu Y, Li Y, Xiang L, Cheng B, Hu Y, Jiang X, Wang Z, Wu S, Si L, Yang Q, Xu J, Huang J. The important role of glycerophospholipid metabolism in the protective effects of polyphenol-enriched Tartary buckwheat extract against alcoholic liver disease. Food Funct. 2022;13:10415–25. https://doi.org/10.1039/d2fo01518h.
58. Xu X, Wang J, Xu L, Li P, Jiang P. p53 suppresses lipid droplet-fueled tumorigenesis through phosphatidylcholine. J Clin Invest. 2024;134:e171788. https://doi.org/10.1172/JCI171788.
59. Lianqun J, Xing J, Yixin M, Si C, Xiaoming L, Nan S, Guoyuan S, Yuan C, Ning Y, Yao W, Na Z, Kaixuan Z, Guanlin Y. Comprehensive multiomics analysis of the effect of ginsenoside Rb1 on hyperlipidemia. Aging. 2021;13:9732–47. https://doi.org/10.18632/aging.202728.
60. Sanchez-Lopez E, Zhong Z, Stubelius A, Sweeney SR, Booshehri LM, Antonucci L, Liu-Bryan R, Lodi A, Terkeltaub R, Lacal JC, Murphy AN, Hoffman HM, Tiziani S, Guma M, Karin M. Choline uptake and metabolism modulate macrophage IL-1β and IL-18 production. Cell Metab. 2019;29:1350–e13621357. https://doi.org/10.1016/j.cmet.2019.03.011.
61. Miura H, Mizuguchi H, Amano-Iwashita M, Maeda-Kogure R, Negishi A, Sakai A, Toyama T, Kawai H, Mitsumoto A, Kudo N. Clofibric acid increases molecular species of phosphatidylethanolamine containing arachidonic acid for biogenesis of peroxisomal membranes in peroxisome proliferation in the liver, biochim. Biophys Acta Mol Cell Biol Lipids. 2021;1866:158963. https://doi.org/10.1016/j.bbalip.2021.158963.
62. van der Veen JN, Kennelly JP, Wan S, Vance JE, Vance DE, Jacobs RL. The critical role of phosphatidylcholine and phosphatidylethanolamine metabolism in health and disease. Biochim Biophys Acta (BBA) Biomembr. 2017;1859:1558–72. https://doi.org/10.1016/j.bbamem.2017.04.006.
63. Yu Z, Yan C, Qiu D, Zhang X, Wen C, Dong S. Accumulation and ecotoxicological effects induced by combined exposure of different sized polyethylene microplastics and Oxytetracycline in zebrafish. Environ Pollut. 2023;319:120977. https://doi.org/10.1016/j.envpol.2022.120977.
64. Chen X, Zhuang J, Chen Q, Xu L, Yue X, Qiao D. Chronic exposure to Polyvinyl chloride microplastics induces liver injury and gut microbiota dysbiosis based on the integration of liver transcriptome profiles and full-length 16S rRNA sequencing data. Sci Total Environ. 2022;839:155984. https://doi.org/10.1016/j.scitotenv.2022.155984.
65. Elfaki I, Mir R, Almutairi F, Duhier F. Cytochrome P450: polymorphisms and roles in cancer, diabetes and atherosclerosis. Asian Pac J Cancer Prev. 2018;19:2057–70. https://doi.org/10.22034/APJCP.2018.19.8.2057.
66. Li J. Research progress on the CYP2B subfamily genes in mammals. Guangdong Chem Ind. 2020;47:103–4.
67. Limonta G, Mancia A, Abelli L, Fossi MC, Caliani I, Panti C. Effects of microplastics on head kidney gene expression and enzymatic biomarkers in adult zebrafish. Comp Biochem Physiol C Toxicol Pharmacol. 2021;245:109037. https://doi.org/10.1016/j.cbpc.2021.109037.
68. Huang Y, Ding J, Zhang G, Liu S, Zou H, Wang Z, Zhu W, Geng J. Interactive effects of microplastics and selected pharmaceuticals on red tilapia: role of microplastic aging. Sci Total Environ. 2021;752:142256. https://doi.org/10.1016/j.scitotenv.2020.142256.
69. Li X, Luo J, Han C, Lu X. Nanoplastics enhance the intestinal damage and genotoxicity of sulfamethoxazole to Medaka juveniles (Oryzias melastigma) in coastal environment. Sci Total Environ. 2023;894:164943. https://doi.org/10.1016/j.scitotenv.2023.164943.
70. He Q. Study on the reproductive toxicity of microplastic exposure in male mice, in: Proceedings of the 10th National Congress of Toxicology of the Chinese Society of Toxicology, Zunyi Medical University, 2023.
71. Goldstein JA. Clinical relevance of genetic polymorphisms in the human CYP2C subfamily, Br. J Clin Pharmacol. 2001;52:349–55. https://doi.org/10.1046/j.0306-5251.2001.01499.x.
72. Roussel F, Marie S, Cresteil T. Gene structure and promoter analysis of the rat constitutive CYP2C23 gene. DNA Cell Biol. 1995;14:777–88. https://doi.org/10.1089/dna.1995.14.777.
73. Kawamura T, Ichikawa M, Hatogai J, Koyama Y, Tachibana M, Kuwahara M, Negishi K, Matsumoto M, Miyazaki M, Ochiai W. Mouse Cyp2c expression and zonation structure in the liver begins in the early neonatal stage. Biopharm Drug Dispos. 2022;43:130–9. https://doi.org/10.1002/bdd.2324.
74. Shoieb SM, Alammari AH, Levasseur J, Silver H, Dyck JRB, El-Kadi AOS. Ameliorative role of fluconazole against abdominal aortic constriction–induced cardiac hypertrophy in rats. J Cardiovasc Pharmacol. 2022;79:833–45. https://doi.org/10.1097/fjc.0000000000001258.
75. Ma F, Lin F, Chen C, Cheng J, Zeldin DC, Wang Y, Wang DW. Indapamide lowers blood pressure by increasing production of epoxyeicosatrienoic acids in the kidney. Mol Pharmacol. 2013;84:286–95. https://doi.org/10.1124/mol.113.085878.
76. Alhashim A, Abdelbary M, Sullivan JC, Naeini SE, Elmarakby AA. Sexual dimorphism in renal Heme oxygenase-1 and arachidonic acid metabolizing enzymes in spontaneously hypertensive rats versus normotensive Wistar Kyoto rats. Prostaglandins Other Lipid Mediat. 2022;161:106650. https://doi.org/10.1016/j.prostaglandins.2022.106650.
77. Tsao CC, Foley J, Coulter SJ, Maronpot R, Zeldin DC, Goldstein JA. CYP2C40, a unique arachidonic acid 16-hydroxylase, is the major CYP2C in murine intestinal tract. Mol Pharmacol. 2000;58:279–87. https://doi.org/10.1124/mol.58.2.279.

Publisher's note

Springer Nature remains neutral with regard to jurisdictional claims in published maps and institutional affiliations.